J Mater Sci (2018) 53:9598–9610

Electronic materials

Photoactive multi-walled carbon nanotubes: synthesis and utilization of benzoin functional MWCNTs

Neşe Kaynak[1], Ayşen Önen[2,*], and Müfide Karahasanoğlu[1]

[1] Department of Polymer Science and Technology, Istanbul Technical University, 34469 Maslak, Istanbul, Turkey
[2] Department of Chemistry, Istanbul Technical University, 34469 Maslak, Istanbul, Turkey

Received: 4 December 2017
Accepted: 16 March 2018
Published online: 26 March 2018

ABSTRACT

This study describes a facile method for the synthesis of functionalized multi-walled carbon nanotubes (MWCNTs) carrying photoactive group. The synthesis of MWCNTs-based macro-photoinitiator was achieved by the esterification reaction between benzoin moiety and acyl chloride functional MWCNTs. Synthesized MWCNT-based photoinitiator (MWCNTs–benzoin) was used in the photopolymerization of styrene to yield polystyrene (PS)-grafted MWCNTs (MWCNTs–PS) by "grafting from" method. The efficiency of MWCNTs–benzoin photoinitiator was determined by evaluating the effect of initiator to monomer ratio and reaction period on photopolymerization of styrene. Fourier transform infrared spectroscopy, Raman and X-ray photoelectron spectroscopy analyses confirmed the covalent bonding for functionalization of MWCNTs and determined the final structures. Thermogravimetric analysis, gel permeation chromatography and UV spectroscopy were performed to evaluate the grafting efficiency of PS that covalently grafted to MWCNTs, and high efficiency of MWCNTs–benzoin as a macro-photoinitiator was also confirmed. Scanning electron microscopy was used to determine the surface morphology of functionalized MWCNTs and MWCNTs–PS.

Introduction

Carbon nanotubes (CNTs) with very different structure properties compared to their allotropic carbon species such as graphite or fullerenes have been accepted as exciting and novel molecular form of carbon since their discovery by Iijima [1]. CNTs have drawn significant attention in sub-branch of nanotechnology due to an extraordinary combination of thermal, mechanical and electrical properties [2–4]. Multi-walled carbon nanotubes (MWCNTs) are composed of multiple concentric rolled up graphene sheets, while single-walled carbon nanotubes (SWCNTs) as the other basic form of CNTs consist of a single cylindrical sheets of graphene [5–8]. Possessing inner and outer doping of tubes, MWCNTs have some advantages over simple SWCNTs, such as higher stability and stiffness. Their unique properties make them very attractive in

Address correspondence to E-mail: onen@itu.edu.tr

https://doi.org/10.1007/s10853-018-2233-4

different fields of applications such as material sciences, electronics, optics, physics and medicine [9–12].

However, the insolubility and low dispersion of MWCNTs in solvents, combined with their high hydrophobicity and poor chemical compatibility, restrict the direct use of them in practical applications. Therefore, both covalent and non-covalent modifications and functionalization strategies have been used to tailor the surface of MWCNTs [13–16]. The attachment of molecules and polymers onto MWCNTs, preferably by covalent interactions, has been used not only to enhance dispensability and processability of MWCNTs in different environments, but also to improve chemical interactions with polymer matrix [17–21].

Among the various types of covalent modification strategies, incorporating carbonyl derivatives onto the surface of MWCNTs is one of the most versatile methods that enables further modification opportunities through ester, amide, etc., groups. Refluxing with concentrated sulfuric and nitric acid is the most common oxidative treatment method to functionalize MWCNTs with carboxylic acid group. The same oxidative treatments are also used to remove amorphous carbon and metallic impurities from pristine MWCNTs [22–25].

Possessing superior properties of MWCNTs and advantageous features of polymers, carbon nanotube–polymer composites have drawn much attention in research and practice [26–32]. "Grafting from" and "grafting to" are two main methods through which covalent attachment of polymer chains on the surface of CNTs can be achieved. The "grafting to" route involves bonding of a preformed end-functionalized polymer chain with the functional groups of CNTs [33–36]. The "grafting from" method is based on covalent immobilization of polymer precursors on CNTs and the addition of appropriate monomers afterward, as propagation step [37–41].

Since it was discovered by Dupont, photoinitiated polymerization has become an important industrial process [42]. Photoinitiators (PIs) have a significant role on the development of this technology. The most important properties of type I PIs are high absorption at far UV region and having high quantum yield during propagation of the radicals. Benzoin and its derivatives are well-known type I PIs, which are also used in commercial applications for UV curable coatings [43–45]. The process is based on the polymerization of appropriate monomers by photochemically generated alkoxy benzyl and benzoyl radicals as shown in Fig. 1.

This article describes the surface functionalization of MWCNTs via photoactive benzoin groups, which can be utilized as a photoinitiator along with its improved dispersion and processability in comparison to pristine MWCNTs. In the following step, benzoin functional MWCNTs (MWCNTs–benzoin) were employed as macro-photoinitiators for the free radical polymerization of styrene to obtain polymer-bounded MWCNTs, which may combine advantageous properties of both MWCNTs and polymers in the same structure.

Materials and methods

Materials

MWCNTs with the outer diameter of about 25–30 nm (provided by Dr. Mohamed Abdel Salam in King Abdulaziz University) were produced by natural gas catalytic decomposition method over Ni/Al_2O_3. Sulfuric acid (H_2SO_4, Merck), nitric acid (HNO_3, Lachema), thionyl chloride ($SOCl_2$, Merck) and pyridine (Lachema) were used without further purification. Styrene (99%, Kempro Chemicals Corp.) was distilled under reduced pressure before use. Dimethylformamide (Labkim), tetrahydrofuran (Labkim) and all solvents were purified and dried by standard techniques before use. Sodium hydride (NaH, Sigma Aldrich) was stored under nitrogen before use. Benzoin (Acros Organics) and the rest of the chemicals were used without further purification.

Methods

Synthesis of acid chloride functional MWCNTs

Three grams of pristine MWCNTs and 100 mL solution of sulfuric and nitric acid mixture with a volume ratio of 3:1, respectively, were added into a round bottom flask for the oxidation of MWCNTs. MWCNTs/acid mixture flask was sonicated for 15 min in an ultrasonic bath to prevent agglomeration of MWCNTs. Then, the flask was equipped with a reflux condenser and thermometer, and the reaction

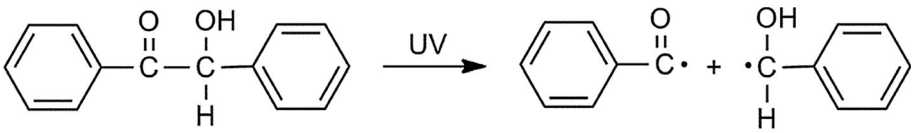

Figure 1 Cleavage of photoactive benzoin initiator.

was carried out under reflux for 2 h. A dense brown gas that evolved through this period was collected and treated with aqueous NaOH that was connected to the condenser. After the reaction was completed and the temperature of the mixture went down to room temperature, the mixture was diluted with distilled water and then vacuum-filtered through a 0.45-μm polytetrafluoroethylene (PTFE) membrane and subsequently washed with distilled water until the pH of the filtrate was approximately 7. The filtered solid was washed with THF and finally dried in vacuum oven at 70 °C giving off MWCNTs–COOH.

For the synthesis of acyl chloride (–COCl) functional MWCNTs, 0.8 g of MWCNTs–COOH were dispersed in 20 mL of anhydrous THF by ultrasonication. Then, 50 ml of $SOCl_2$ and 2 drops of anhydrous DMF were added into a three-necked round bottom flask containing dispersed MWCNTs–COOH in THF. The reaction of acyl chloride functionalization was carried out for 24 h in nitrogen atmosphere under reflux at 75 °C. The resulting solid was then separated by vacuum filtration using a 0.45-μm PTFE membrane filter and subsequently washed with anhydrous THF. The final –COCl functional MWNTs (MWNTs–COCl) were obtained by the removal of solvent residue under vacuum. The oxidation and functionalization reactions are shown schematically in Fig. 2.

Synthesis of benzoin functionalized MWCNTs

0.4 g of MWCNTs–COCl were dispersed in 50 ml of anhydrous THF by ultrasonication. One gram of benzoin and a few drops of pyridine were added into the dispersion. The mixture was stirred in the dark for 48 h under nitrogen protection at 65 °C. The resulting benzoin functional MWCNTs (MWCNTs–benzoin) were separated from the mixture by filtration and washed repeatedly with anhydrous THF to remove the unreacted benzoin. After drying overnight in vacuum, MWCNTs–benzoin was stored in a dark colored, sealed vial. The illustration of the synthesis is shown in Fig. 3.

Polymerization of styrene with MWCNTs–Benzoin photoinitiator

The vial containing the dispersion of MWCNTs–benzoin and styrene in THF solution was degassed with nitrogen in usual manner and irradiated in a UV photoreactor (λ_{max} = 365 nm, medium pressure mercury UV lamp) at 25 °C. At the end of the polymerization, the solution was filtered to separate the polystyrene-bounded MWCNTs, and washed with plenty of THF to completely remove the unbounded polystyrene. MWCNT-bounded polystyrene (MWCNTs–PS) was washed with methanol and dried overnight under vacuum. Illustration of the photopolymerization is shown in Fig. 4.

Defunctionalization of MWCNTs–PS was carried out by the base-catalyzed hydrolysis method [46]. Forty-nine milligrams of MWCNTs–PS was dispersed in 3 ml of anhydrous THF in a round bottom flask, and then 49 mg of NaH was added. The solution was refluxed at 65 °C under nitrogen protection for 2 h. After the solution was cooled down to room temperature, liquid phase containing detached PS was separated from the solid dark colored MWCNTs and subsequently poured into 100 ml of methanol. After the mixture was centrifuged with 4500 rpm at 5 °C, PS was precipitated at the bottom of the glass vial, and the upper solvent layer was carefully decanted. Then, the precipitated detached PS was dried in vacuum.

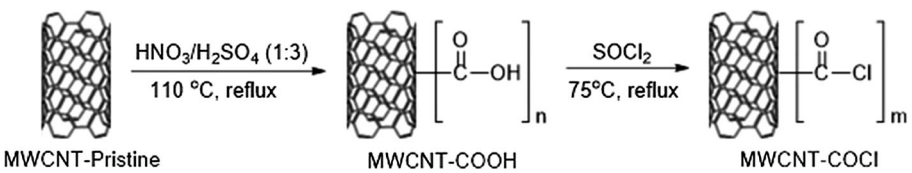

Figure 2 Synthesis of MWCNTs–COOH and MWCNTs–COCl.

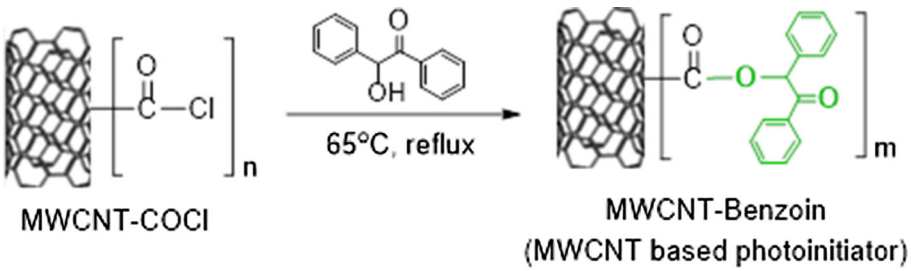

Figure 3 Synthesis of MWCNTs–benzoin.

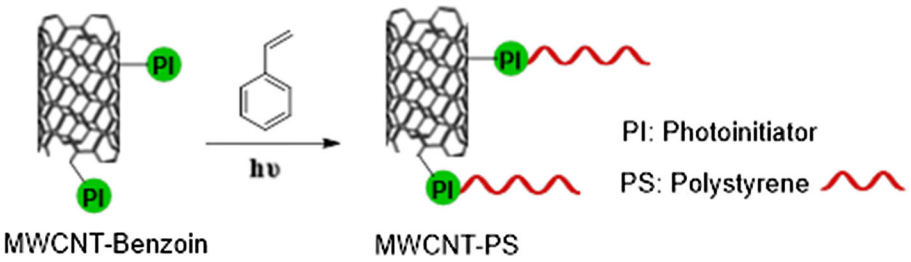

Figure 4 Illustration of the photopolymerization on the surface of MWCNTs–benzoin.

Analysis

Fourier transform infrared (FTIR) analysis was performed on a Nicolet iS10 FTIR spectrometer with 4 cm^{-1} resolution. The spectra were collected from 16 scans for each sample, operating in the frequency range of 4000–400 cm^{-1}.

Raman spectroscopic characterization was carried out on a Renishaw inVia Reflex Raman microscope with a solid-state laser (excitation at 514 nm), grating of 2400 lines/mm at room temperature.

Thermogravimetric analysis (TGA) was performed on a Q50 TGA by TA Instruments under nitrogen atmosphere at a heating rate of 20 °C/min. The weights of samples were about 10 mg in a Pt crucible.

X-ray photoelectron spectrometer (XPS) measurements were performed on a Thermo-Scientific spectrometer with monochromatic AlK-α photon source under ultra-high vacuum ($P < 5 \times 10^{-9}$ mbar). During XPS spectra process, the pass energy was set to 100 eV corresponding to a spectral resolution of about 0.1 eV. Flood gun was used during the measurements for charging compensation.

Molecular weight and polydispersity of PS were analyzed by Agilent 1100 Series Gel Permeation Chromatography (GPC) equipped with RI-G1362A refractive index detector. Tetrahydrofuran (THF) was used as the eluent with a flow rate of 0.5 mL/min at 30 °C, and polystyrene was used as standards.

UV–vis–NIR absorption spectra were recorded with a UV-1700 spectrometer (Schimadzu) operating between 200 and 800 nm. Samples were prepared after the sonicating process and diluted by a certain factor, resulting in certain MWCNT contents that were suitable for UV–vis measurements.

Morphological surface properties of MWCNTs were observed by an EVO MA10 scanning electron microscope (SEM) with a tungsten filament by Zeiss.

Results and discussion

In this study, MWCNTs were modified with –COCl over –COOH functionality. Subsequently, chloride functional MWCNTs (MWCNTs–COCl) reacted with benzoin moiety yielding photoactive MWCNT–benzoin by esterification reaction. In the second stage, MWCNT–benzoin macro-photoinitiators were employed to initiate the polymerization of styrene under UV irradiation.

FTIR analysis was performed to characterize the chemical structure of functionalized MWCNTs with the dispersed samples in THF. The reason for preparing dispersions is the black color of MWCNTs which has the absorbing property for all infrared rays resulting in difficulty for FTIR analysis. Characteristic absorption peaks of MWCNTs–pristine, MWCNT–COOH and MWCNT–benzoin are shown in the spectra of Fig. 5.

The weak peak related to C=C aromatic ring stretching and phonon modes (ketone, quinone and derivatives) of MWCNTs is observed at 1640 cm^{-1} in the FTIR spectra of the all samples [47]. Noticeable peaks at 2850–3000 cm^{-1} were assigned to C–H

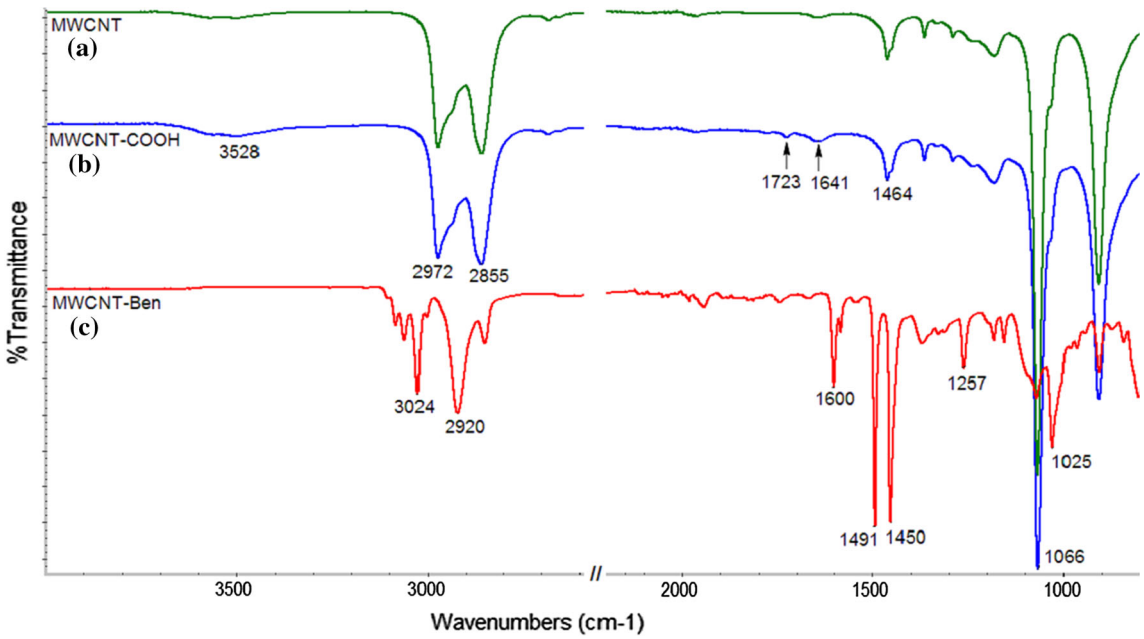

Figure 5 FTIR spectra of **a** MWCNT–pristine, **b** MWCNT–COOH and **c** MWCNT–benzoin.

asymmetric and symmetric stretching vibrations. The weak broad peak around 3528 cm^{-1} in spectrum (A) is assigned to the vibration of O–H group in MWCNTs–pristine. It is likely to observe related absorption peaks of some minor functional groups of MWCNTs–pristine. Such functional groups may be originated from carbonaceous fragments and possible partial oxidation related to purification methods and storage conditions of MWCNT–pristine [48].

Compared to the spectra of MWCNTs–pristine, the increasing intensity of broad O–H absorption in MWCNT–COOH spectra (B) and the appearance of a weak peak at 1723 cm^{-1}, which is characteristic of –COOH, confirm the carboxyl functionality of MWCNT–COOH. The disappearance of broad OH absorption around 3528 cm^{-1} and the appearance of a new peak at 1600 cm^{-1} in Fig. 5c both indicate the esterification reaction between –COOH group of MWCNTs–COOH and –OH group of benzoin molecule confirming the covalent attachment of benzoin moiety in MWCNTs.

Raman spectroscopy is a very valuable tool for the characterization of carbon-based nanostructures. The structure of MWCNTs and the functionalization on the surface were also studied by Raman spectroscopy. The spectra of pristine and functional MWCNTs in the range of 1000–1800 cm^{-1} frequency are shown in Fig. 6. Each spectrum consists of three common characteristic bands assigned as D-band at

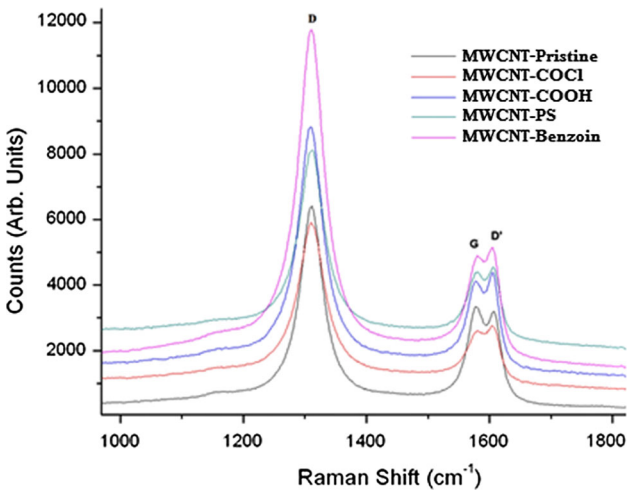

Figure 6 Raman spectra of pristine and functionalized MWCNTs.

$\sim$ 1310 cm^{-1}, G-band at 1580 cm^{-1} and D′-band at 1617 cm^{-1}. D-band corresponds to double resonance effects in carbon and is attributed to the presence of disordered amorphous carbon [7, 49]. It is important to mention that carbon structural disorder is due to the structural imperfections such as impurities, nanosized graphitic planes and any other forms of carbon. Thus, D-band mode (ill-organized graphitic) should not be considered directly related to the defects in the tube walls. G-band corresponds to the tangential C–C bond vibrations of hexagonal carbon

in graphene sheets. In addition, as seen in Table 1, D′ band is also related to the double resonance feature induced by strain in C–C bond vibrations and disorder due to the defects and functionalization.

The intensity ratios of the D–G band (I_D/I_G) can be seen as a proof of disruption in the aromatic π-electrons system of CNTs. The I_D/I_G for functionalized MWCNTs are higher than that of the MWNTs–pristine. This result indicated that a number of sp^2 hybridized carbons were converted to sp^3 hybridization carbons caused by the covalent functionalization of MWCNTs. In addition, when functionalization occurs the intensity of D′ band is higher than the G band, as a result of increasing disorder.

The chemical composition of the surface of MWCNT samples was also analyzed by XPS, which is one of the surface analytical techniques providing information about the nature of the functional groups and also about the presence of structural defects on the MWCNTs surface [50]. XPS spectra were obtained in the regions of the main elements of interest (C, O and Cl), and Figure 7 presents the XPS spectra of pristine and functionalized MWCNTs. All samples showed photoemission peaks around 284.0 eV and 533.0 eV corresponding to typically C and O atoms in 1 s configurations, and both samples of MWCNTs–COCl and MWCNTs–benzoin showed weak peaks at ~ 200 eV for Cl atom in 2p configuration. The existence of oxygen in MWCNTs–pristine may be related to oxide catalyst residues of MWCNTs, or/and any possible oxygen containing impurities in MWCNTs–pristine. The O atom observation in MWCNTs–pristine by XPS is also in agreement with FTIR analysis and TGA of MWCNTs–pristine which will be discussed in a later part.

The atomic concentrations of the surface elements of MWCNTs and their relative ratios evaluated by quantitative analysis of XPS are also provided in Table 2. MWCNTs–COOH presented a highly increased amount of oxygen (12.28%) due to attached –COOH functionality. The appearance of a new Cl atom signal in the XPS spectra of MWCNTs–COCl

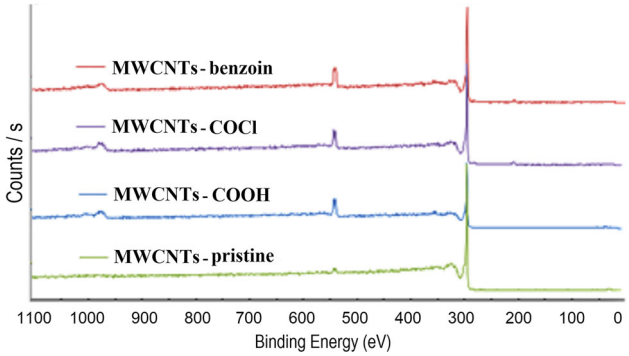

Figure 7 XPS image of MWCNT–pristine, MWCNTs–COOH, MWCNTs–COCl and MWCNTs–benzoin.

indicated that chemical composition was changed on the surface of MWCNTs during covalent functionalization. Comparing the ratios of O and Cl atoms to C atom (O/C: 0.1 and Cl/C:0.019) for MWCNTs–COCl sample, relatively small amount of Cl (1.66%) may indicate that –COCl functionalization did not occur in a high yield. However, –COCl is a very reactive functional group and can easily be transformed to –COOH functionality. Thus, the possible transformation of –COCl before or/and during the XPS measurement might have decreased the amount of Cl atom while increasing the amount of O atom on the surface of MWCNTs. Beside, we have the evidence of oxygen trace for pristine MWCNTs as we already discussed. By the quantitative analysis of XPS of MWCNTs–benzoin, it is presented in Table 2 that O atom reached 14.22% related to benzoin molecule. The significant decrease in the amount of Cl atom for MWCNTs–benzoin also confirms the attachment of benzoin moiety, while the remaining small amount of Cl atoms indicates the difficulty of chloride functionality to react with benzoin due to the steric hindrance of benzoin molecule.

TGA analysis was applied to examine the thermal stability of MWCNTs samples and to investigate the content of functional MWCNTs. The samples were heated up to 800 °C with a heating rate of 20 °C/min under nitrogen, and the spectra of MWCNT–pristine,

Table 1 I_D/I_G and $I_{D'}/I_G$ intensity ratios for the pristine and functional MWCNTs

Sample	MWCNT–Pristine	MWCNT–COOH	MWCNT–COCl	MWCNT–Benzoin	MWCNT–PS
I_D/I_G	2.08	3.00	3.55	3.58	3.14
$I_{D'}/I_G$	0.96	1.10	1.15	1.11	1.14

Table 2 Chemical composition (%) and ratios of MWCNTs determined by XPS

Sample	C1s (%)	O1s (%)	Cl2p (%)	O/C	Cl/C
MWCNTs–Pristine	97.91	2.08	–	0.021	–
MWCNTs–COOH	87.72	12.28	–	0.140	–
MWCNTs–COCl	89.36	8.97	1.66	0.100	0.019
MWCNTs–Benzoin	85.15	14.22	0.63	0.167	0.007

MWCNTs–COOH, MWCNTs–COCl and MWCNTs–benzoin are presented in Fig. 8. It is well known that different structural forms of carbon can exhibit different thermal stability depending on its oxidation behavior [50]. Such as, disordered or amorphous carbons tend to be oxidized at around 500 °C, whereas a well-graphitized structures may start to oxidize above 600 °C depending on the type of CNTs. MWCNTs–pristine showed a major decomposition at 550 °C, and the weight loss occurred up to 800 °C was ~ 7% corresponding to disordered carbon due to thermal oxidation. The small mass loss of MWCNTs–pristine is also due to possible oxygen groups, and the defects occurred on the carbon structure. The existence of oxygen despite the inert TGA atmosphere is likely due to the formation and purification process of MWCNTs and is consistent with the FTIR and XPS results, which are both indicating oxygen trace. The observed mass loss up to 180 °C is associated with the release of water which is physically or chemically absorbed and was less than 0.3% for MWCNT–pristine. The higher amount of mass losses up to 180 °C for functional MWCNTs are also associated with the release of water along with the release of possible volatile residues [38].

The thermal stage between the temperatures of 180 and 550 °C as seen in Fig. 8 is attributed to pyrolysis of organic functionalities of MWCNTs. The observed mass loss between 180 and 550 °C is less than 1% for MWCNT–pristine, and the mass losses for the same temperature range are 8.39, 12.14 and 22.29% for MWCNTs–COOH, MWCNTs–COCl and MWCNTs–benzoin, respectively. Relative moles of covalently attached functional groups were calculated by the following equation according to the weight losses (% W_{loss}) between 180 and 550 °C; ($\eta_{grafting/g}$ = % W_{loss}/ 100 × $MW_{organic\ component}$). Taking the molecular weight of –COOH group into account, the weight loss of 8.39% for MWCNTs–COOH indicates ~ 2.1 mmol of –COOH functionality for per gram of MWCNTs–COOH. Estimated by the related equation considering the molecular weights of attached organic units, weight losses of corresponding organic functionalities of MWCNTs indicate that almost all –COOH unit (–COOH:C atom; 1:36) was transformed to –COCl functionality for MWCNTs–COCl and ~ 50% of

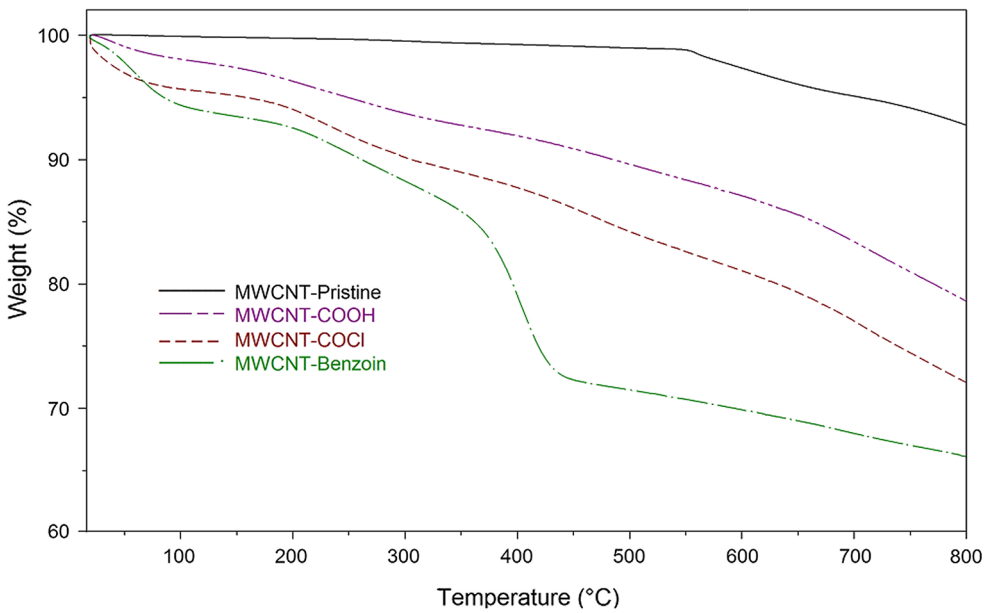

Figure 8 TGA curves of MWCNT–pristine, MWCNTs–COOH, MWCNTs–COCl and MWCNTs–benzoin.

–COCl units were reacted with benzoin molecule resulting in MWCNTs–benzoin (benzoin:carbon atom; 1:80). The ratio of attached benzoin is expectable considering the possible steric hindrance of benzoin molecule for the reaction and is well acceptable for a photoinitiator.

Following the synthesis and structural determination of MWCNTs–benzoin as macro-photoinitiator, covalent grafting of polystyrene to MWCNTs was achieved by polymerization of styrene under UV irradiation. Photoactive benzoin decomposes under UV irradiation and forms two free radicals, namely alkoxy benzyl and benzoyl radicals both of which are effective. In our case, it might appear necessary for MWCNT-bounded alkoxy benzyl radical to initiate styrene polymerization instead of benzoyl radical. However, in the case of monomers like styrene which prefers termination mainly by combination, MWCNT-bounded alkoxy benzyl radicals can also act in the termination step by coupling with the propagating radicals derived from either benzoyl or alkoxy benzyl radicals. Thus, MWCNTs-bounded polystyrene (MWCNTs–PS) was highly expectable beside some free-unbounded PS.

In order to investigate the role and the efficiency of MWCNT–benzoin as a macro-photoinitiator, polymerizations of styrene in the presence of MWCNT–benzoin were performed under UV irradiation with different weight ratios of styrene monomer/MWCNT–benzoin initiator (R). For this purpose, polymerizations with the R of 10, 20 and 45 were performed representing the resulted PS-grafted MWCNTs as MWCNTs–10PS, MWCNTs–20PS and also with the constant R of 45 in different UV irradiation periods of 1 h, 2 h and 3 h representing the products as MWCNTs–45PS1, MWCNTs–45PS2, MWCNTs–45PS3, respectively.

Covalently bounded PS was separated from MWCNTs in order to characterize the grafted PS and determine the molecular weight of PS. The grafted PS, detached from the surface of MWCNTs–PS, was prepared for GPC analysis by precipitating into methanol and dissolving in THF afterward. The number-average molecular weights (M_n) of detached PS with R values of 10 and 20 (MWCNTs–10PS and MWCNTs–20PS) could not be detected by GPC indicating very low M_n of grafted PS. M_n values of detached PS from MWCNTs–45PS were also determined by GPC, and the results including polydispersity index (PDI) are given in Table 3. Contrary to undetectable M_n values of PS from both MWCNTs–10PS and MWCNTs–20PS, high M_n values of PS from MWCNTs–45PS expressed the effect of low and high values of monomer to initiator ratio (R), resulting in low M_n of short polymer chains and higher M_n of longer polymer chains, respectively. The results are as expected from the well-known mechanism of free radical polymerization. As presented in Table 3, the high PDI values of MWCNTs–45PS are also consistent with the free radical polymerization mechanism. Thus, the results evaluated from the GPC analysis confirmed the role of MWCNT–benzoin as a macro-photoinitiator and signified the high efficiency of MWCNT–benzoin for the grafting polymerization of styrene from the surface of MWCNTs.

TGA analysis was also applied to quantify PS grafting degree of MWCNTs–PS and examine the thermal stability of the samples. Figure 9 displays the TGA curves of MWCNTs–45PS1, MWCNTs–45PS2, MWCNTs–45PS3 along with the curves of detached PS (homo polystyrene) from MWCNTs–45PS3 and MWCNTs–pristine as reference.

As seen in Fig. 9, MWCNTs–pristine showed major decomposition at 550 °C, and detached PS (homo polystyrene) displayed major decomposition stage between 371 and 500 °C reaching total mass loss at 550 °C. Analyzing the curves of MWCNTs–45PS1, MWCNTs–45PS2 and MWCNTs–45PS3, major decompositions were also observed at about 372 °C being almost the same as PS indicating that MWCNTs did not have a significant effect on the decomposition temperature of MWCNTs–PS.

Mass loss of MWCNTs–pristine and PS were less than 1 and 0.3% at 550 and 370 °C, respectively. The observed mass losses up to 180 °C for all samples were associated with the release of water and possible volatile residues. The small organic compounds attached to MWCNTs such as –COOH and benzoin were totally decomposed below 350 °C, as discussed in the previous section. Evaluating the results, thermal stage of 350–550 °C is attributed to decomposition stage of grafted PS, and the weight losses of this stage is corresponded to the grafting degree of PS. The observed weight losses between 350 and 550 °C were 19.20%, 22.87 and 78.26 for MWCNTs–45PS1, MWCNTs–45PS2 and MWCNTs–45PS3, respectively, corresponding to grafting percentages of PS on MWCNTs and given as GPS% in Table 3. As determined from the grafting contents of PS, the increase in the UV irradiation period from 1 h to 3 h resulted

Table 3 Photopolymerization of styrene in the presence of MWCNTs–benzoin[a] at 25 °C

Samples	Reaction time (h)	Grafted PS M_n ($\times 10^5$)	GPS[b] %	PDI
MWCNTs–45PS1	1	1.01	19.20	1.95
MWCNTs–45PS2	2	1.18	22.87	2.0
MWCNTs–45PS3	3	1.45	78.26	1.75

MWCNTs–benzoin[a] = with the R of 45, the weight ratio of styrene/MWCNTs–benzoin

GPS[b] (%) = Mass percentage of the grafted PS calculated from TGA

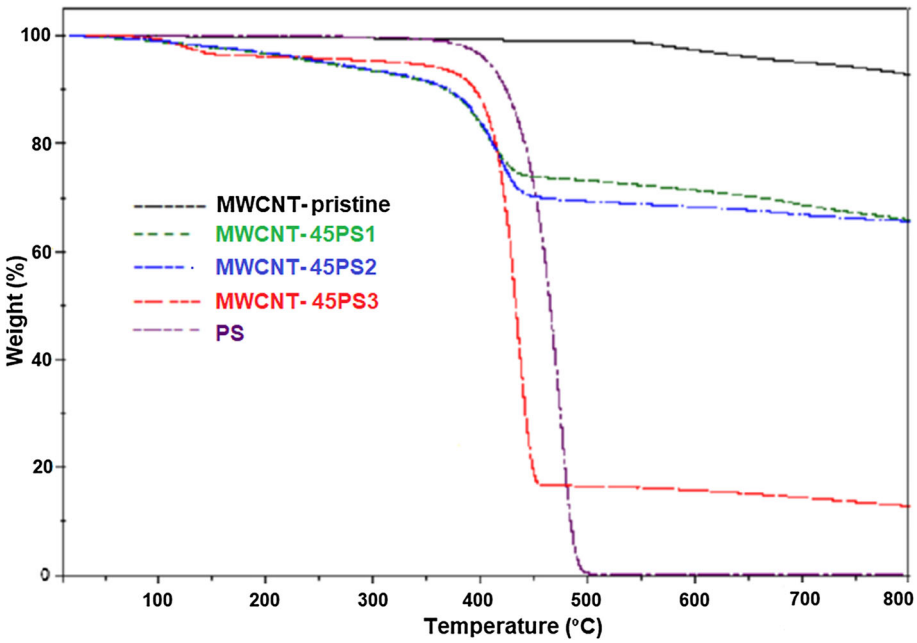

Figure 9 TGA curves of MWCNT–pristine, MWCNTs–45PS1, MWCNTs–45PS2, MWCNTs–45PS3 and homo PS.

in the increase in polymerization yield of styrene on MWCNTs despite the similar molecular weights of PS obtained by GPC. The results, well consistent with the results of GPC analysis, are in a good agreement with the free radical mechanism of UV polymerization in which irradiation time does not have a significant effect on M_n but effects the yield of obtained polymer. TGA also confirmed the macro-photoinitiator property of MWCNT–benzoin and its efficiency for the polymerization of styrene.

The effect of functionalization on the surface morphology of MWCNTs was analyzed by SEM, and the observed images are shown in Fig. 10. MWCNTs were clearly observed lying on the gold layer by 50000 magnifications. MWCNTs–pristine exhibited nanowire-like morphology and a smooth surface with nothing adhering to them (Fig. 10a). The nanowire-like morphology can also be observed on functional MWCNTs same as on MWCNTs–pristine, except the space between nanowires becoming smaller. The oxidation of MWCNTs by strong acid treatment significantly alters the surface roughness of the nanotubes and also reduces the length of nanotubes as observed for MWCNTs–COOH in Fig. 10b. The existence of functional groups on the surface of MWCNTs resulted in the increase in the average diameter of the MWCNTs [51]. The rods became less distinct for MWCNTs–PS (Fig. 10d) due to the fact that MWCNTs were enclosed with polystyrene.

UV absorption spectra of MWCNTs–PS, MWCNTs–COOH and detached PS of MWCNTs–PS during UV radiation were examined and are presented in Fig. 11. The characteristic absorption band of PS obtained from the defunctionalization reaction of MWCNTs–PS was observed at ~ 260 nm corresponding to absorption band of phenyl groups. The spectrum of MWNTs–COOH did not exhibit any significant absorption, while that of MWNTs–PS exhibited absorption band similar to the detached PS of MWCNTs–PS.

Dispersion behavior of functional MWCNTs in THF was observed. Figure 12 shows three vials

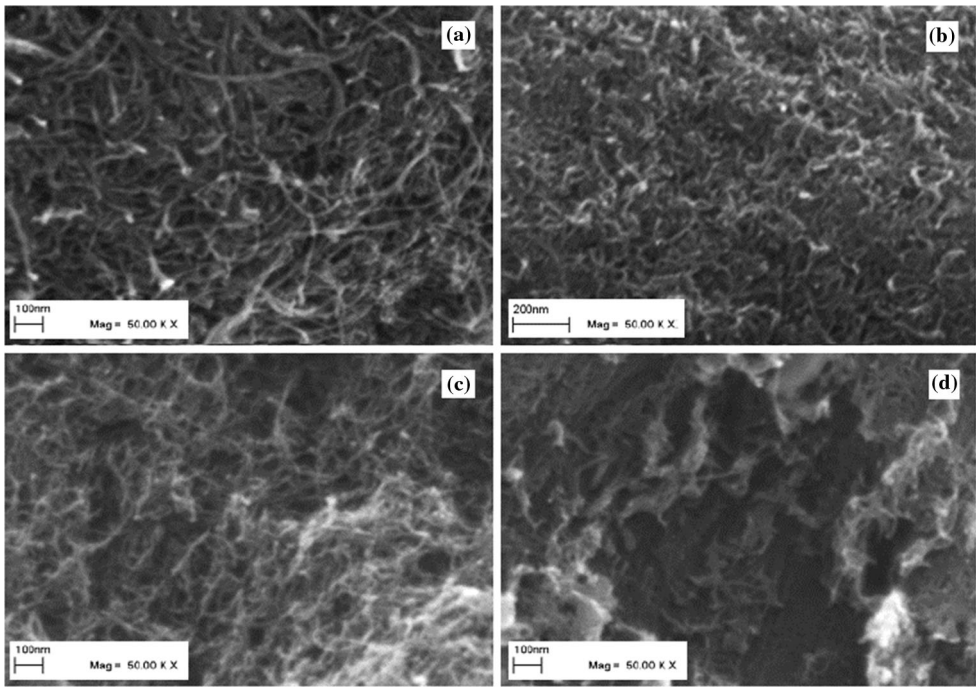

Figure 10 SEM images of pristine MWCNT (**a**), MWCNTs–COOH (**b**), MWCNTs–benzoin (**c**) and MWCNTs–45PS2 (**d**).

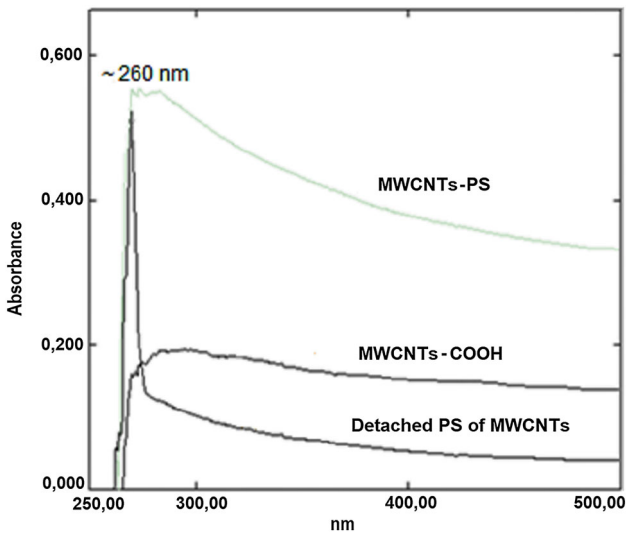

Figure 11 UV–Vis absorption spectra of MWCNTs–PS, MWCNTs–COOH and detached PS.

containing equal masses of MWCNTs–pristine, MWCNTs–COOH and MWCNTs–45PS2 separately in equal volumes of THF. Obviously, MWCNTs–pristine was not dispersed in THF. Organic functionalities of MWCNTs increased dispersion and solubility of both MWCNTs–COOH and MWCNTs–45PS2 as expected. MWCNTs–COOH dispersion in THF did not collapse for the first 6 h, and then it started to settle down. MWCNTs–PS in THF formed

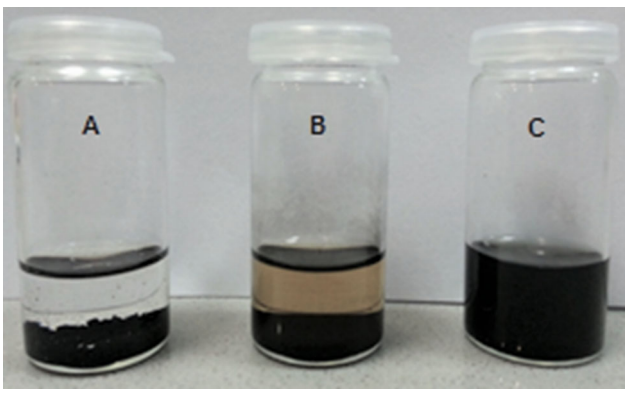

Figure 12 Dispersion behavior of **a** MWCNTs–pristine, **b** MWCNTs–COOH, **c** MWCNTs–45PS2 in THF after a storage of 1 week.

a clear, black solution that exhibited no discernible particulate material and remained stable for a period of at least 1 week.

Conclusions

In the present study, the attempt was to design a MWCNTs-based photoinitiator and determine its efficiency in photopolymerization of styrene via "grafting from" method. Functionalization of MWCNTs as a macro-photoinitiator was achieved by the esterification reaction between acid chloride

functional MWCNTs (MWCNTs–Cl) and benzoin moiety. The expected structure of synthesized benzoin functional MWCNTs (MWCNTs–benzoin) was confirmed by FTIR, Raman, XPS and TGA analysis.

The well-designed MWCNTs–benzoin as a macrophotoinitiator enabled the polymerization of styrene (MWCNTs–PS) grafting from MWCNTs under UV irradiation. Defunctionalization of MWCNTs–PS was also performed by hydrolysis for the further characterization of detached PS of MWCNTs. Characterization of MWCNTs–PS by GPC, TGA and UV absorption analysis well confirmed that PS component was covalently grafted from MWCNTs.

The efficiency of MWCNTs–benzoin for photopolymerization was investigated by performing polymerizations with different weight ratios (R) of styrene/MWCNT–benzoin and in different UV irradiation periods. The values of molecular weights (M_n), polymerization yields and polydispersity index (PDI) of PS grafted from MWCNTs were obtained from the consistent results of GPC and TGA. GPC results clearly indicated that MWCNTs–PS with detectable M_n could not be obtained by lower styrene/MWCNTs–benzoin weight ratios (R: 10 and 20), whereas higher styrene/MWCNTs–benzoin weight ratio (R:45) resulted in grafted PS with M_n of about 1.45×10^5, which is truly supported by the well-known effect of monomer/initiator concentration on the M_n of a polymer.

Moreover, the increase in the UV irradiation period, from 2 to 3 h, resulted in a slight increase in M_n of grafted PS, from 1.18×10^5 to 1.45×10^5, whereas increasing the UV irradiation period resulted in a dramatic increase in the grafting yields of PS, from 22.87 to 78.26%. This result is also in very good agreement with the well-known mechanism of UV initiated free radical polymerization in which the increase in irradiation time does not significantly affect the molecular weight of polymer but increase the yield of the resulting polymer. Thus, it is strongly confirmed that MWCNTs–benzoin was successfully synthesized, and act as an effective initiator for the photopolymerization of styrene.

SEM images of functionalized and PS-grafted MWCNTs indicated the increase in the average diameter of MWCNTs with the increasing content of organic grafting. Since the MWCNTs were completely enclosed with PS, the rods between the MWCNTs became less distinct. Dispersion behavior of MWCNTs in THF was also examined, and it was observed as expected that stability and dispersion ability of MWCNTs–PS were higher than those of MWCNTs–pristine and MWCNTs–COOH in THF.

Compliance with ethical standards

Conflict of interest There is no conflict of interest between the authors of this manuscript.

References

[1] Iijima S (1991) Helical microtubules of graphitic carbon. Nature 354:56–58

[2] Dresselhaus MS, Dresselhaus G, Charlier JC, Hernandez E (2004) Electronic, thermal and mechanical properties of carbon nanotubes. Philos Trans A Math Phys Eng Sci 362:2065–2098

[3] Tang Y, Allen BL, Kauffman DR, Star A (2009) Electrocatalytic activity of nitrogen-doped carbon nanotube cups. J Am Chem Soc 131:13200–13201

[4] Tasis D, Tagmatarchis N, Bianco A, Prato M (2006) Chemistry of carbon nanotubes. Chem Rev 106:1105–1136

[5] Prasek J, Drbohlavova J, Chomoucka J, Hubalek J, Jasek O, Adam V, Kizek R (2011) Methods for carbon nanotubes synthesis—review. J Mater Chem 21:15872–15884

[6] Belin T, Epron F (2005) Characterization methods of carbon nanotubes: a review. Mater Sci Eng B119:105–118

[7] Lehman JH, Terrones M, Mansfield E, Hurst KE, Meunier V (2011) Evaluating the characteristics of multiwall carbon nanotubes. Carbon 49:2581–2602

[8] Niyogi S, Hamon MA, Hu H, Zhao B, Bhowmik P, Sen R, Itkis ME, Haddon RC (2002) Chemistry of single-walled carbon nanotubes. Acc Chem Res 35:1105–1113

[9] Spitalsky Z, Tasis D, Papagelis K, Galiotis C (2010) Carbon nanotube–polymer composites: chemistry, processing, mechanical and electrical properties. Prog Polym Sci 35:357–401

[10] Sahoo NG, Rana S, Cho JW, Li L, Chan SH (2010) Polymer nanocomposites based on functionalized carbon nanotubes. Prog Polym Sci 35:837–867

[11] Richard C, Balavoine F, Schultz P, Ebbesen TW, Mioskowski C (2003) Supramolecular self-assembly of lipid derivatives on carbon nanotubes. Science 300:775–778

[12] Martin CR, Kohli P (2003) The emerging field of nanotube biotechnology. Nat Rev 2:29–37

[13] Wepasnick K, Smith B, Bitter J, Fairbrother DH (2010) Chemical and structural characterization of carbon nanotube surfaces. Anal Bioanal Chem 396:1003–1014

[14] Hirsch A (2002) Functionalization of single-walled carbon nanotubes. Angew Chem Int Ed 41:1853–1859

[15] Tasis D, Tagmatarchis N, Georgakilas V, Prato M (2003) Soluble carbon nanotubes. Chem Eur J 9:4000–4008
[16] Dyke CA, Tour JM (2003) Solvent-free functionalization of carbon nanotubes. J Am Chem Soc 125:1156–1157
[17] Qin Y, Liu L, Shi J, Wu W, Zhang J, Guo ZX, Yongfang L, Daoban Z (2003) Large scale preparation of solubilized carbon nanotubes. Chem Mater 15:3256–3260
[18] Grady BP (2010) Recent developments concerning the dispersion of carbon nanotubes in polymers. Macromol Rapid Commun 31:247–257
[19] Li CY, Li L, Cai W, Kodjie SL, Tenneti KK (2005) Nanohybrid shish-kebabs: periodically functionalized carbon nanotubes. Adv Mater 17:1198–1202
[20] Eitan A, Jiang K, Dukes D, Andrews R, Schadler LS (2003) Surface modification of multiwalled carbon nanotubes: toward the tailoring of the interface in polymer composites. Chem Mater 15:3198–3201
[21] Zhao B, Hu H, Haddon RC (2004) Synthesis and properties of a water-soluble single-walled carbon nanotube–poly(m-aminobenzene sulfonic acid) graft copolymer. Adv Funct Mater 14:71–76
[22] Peng H, Alemany LB, Margrave JL, Khabashesku VN (2003) Sidewall carboxylic acid functionalization of single-walled carbon nanotubes. J Am Chem Soc 125:15174–15182
[23] Rosca ID, Watari F, Uo M, Akasaka T (2005) Oxidation of multiwalled carbon nanotubes by nitric acid. Carbon 43:3124–3131
[24] Smith B, Wepasnick K, Schrote KE, Bertele AR, Ball WP, O'Melia C, Fairbrother DH (2009) Colloidal properties of aqueous suspensions of acid-treated, multi-walled carbon nanotubes. Environ Sci Technol 43:819–825
[25] Bergeret C, Cousseau J, Fernandez V, Mevellec J-Y, Lefrant S (2008) Spectroscopic evidence of carbon nanotubes' metallic character loss induced by covalent functionalization via nitric acid purification. J Phys Chem C 112:16411–16416
[26] Moniruzzaman M, Winey KI (2006) Polymer nanocomposites containing carbon nanotubes. Macromolecules 39:5194–5205
[27] Lingling L, Wenjun H, Jun S, Jianjun W, Chuanxiang Q, Lixing D (2014) Preparation of poly (vinyl alcohol) fibers strengthened using multiwalled carbon nanotubes functionalized with tea polyphenols. J Mater Sci 49:3322–3330. https://doi.org/10.1007/s10853-014-8039-0
[28] Gao C, Duan CV, Jin YZ, Li W, Armes SP (2005) Multihydroxy polymer-functionalized carbon nanotubes: synthesis, derivatization, and metal loading. Macromolecules 38:8634–8648
[29] Cheng J, Fernando KAS, Veca LM, Sun Y-P, Lamond AI, Lam YW, Cheng SH (2008) Reversible accumulation of PEGylated singlewalled carbon nanotubes in the mammalian nucleus. ACS Nano 2:2085–2094
[30] Khun NW, Troconis BCR, Frankel GS (2014) Effects of carbon nanotube content on adhesion strength and wear and corrosion resistance of epoxy composite coatings on AA2024-T3. Prog Org Coat 77:72–80
[31] Chen TK, Tien YI, Wei KH (2000) Synthesis and characterization of novel segmented polyurethane/clay nanocomposites. Polymer 41:1345–1353
[32] De Volder MF, Tawfick SH, Baughman RH, Hart AJ (2013) Carbon nanotubes: present and future commercial applications. Science 339:535–539
[33] Akbar S, Beyou E, Cassagnau P, Chaumont P, Farzi G (2009) Radical grafting of polyethylene onto MWCNTs: a model compound. Polymer 50:2535–2543
[34] Pramanik NB, Singha NK (2015) Direct functionalization of multi-walled carbon nanotubes (MWCNTs) via grafting of poly(furfuryl methacrylate) using Diels–Alder "click chemistry" and its thermoreversibility. RSC Adv 5:94321–94327
[35] Yang C, Guenzi M, Cicogna F, Gambarotti C, Filippone G, Pinzino C, Passaglia E, Dintcheva NT et al (2016) Grafting of polymer chains on the surface of carbon nanotubes via nitroxide radical coupling reaction. Polymer 65:48–56
[36] Ernould B, Bertrand O, Minoia A, Lazzaroni R, Vlad A, Gohy JF (2017) Electroactive polymer/carbon nanotube hybrid materials for energy storage synthesized via a "grafting to" approach. RSC Adv 7:17301–17310
[37] Xu Y, Gao C, Kong H, Yan D, Jin YZ, Watts PCP (2004) Growing multihydroxyl hyperbranched polymers on the surfaces of carbon nanotubes by in situ ring-opening polymerization. Macromolecules 37:8846–8853
[38] Luo Y-L, Bai R-X, Xu F, Chen Y-S, Li H, Dai S-S, Ma W-B (2016) Novel multiwalled carbon nanotube grafted with polyethylene glycol-block-polystyrene nanohybrids: ATRP synthesis and detection of benzene vapor. J Mater Sci 51:1363–1375. https://doi.org/10.1007/s10853-015-9455-5
[39] Baskaran D, Mays JW, Bratcher MS (2004) Polymer-grafted multiwalled carbon nanotubes through surface-initiated polymerization. Angew Chem Int Ed 43:2138–2142
[40] Liu Y, Adronov A (2004) Preparation and utilization of catalyst-functionalized single-walled carbon nanotubes for ring-opening metathesis polymerization. Macromolecules 37:4755–4760
[41] Qu L, Veca LM, Lin Y, Kitaygorodskiy A, Chen B, McCall AM, Connell JW, Sun YP (2005) Soluble nylon-functionalized carbon nanotubes from anionic ring-opening polymerization from nanotube surface. Macromolecules 38:10328–10331
[42] Plambeck L Jr (1956) Photographic preparation of relief images. US Patent 2760863

[43] Esen DS, Arsu N, Silva JP, Jockusch S, Turro NJ (2013) Benzoin type photoinitiator for free radical polymerization. J Polym Sci Polym Chem 51:1865–1871

[44] Frick E, Schweigert C, Noble BB, Ernst HA, Lauer A, Liang Y, Dominik V, Coote ML et al (2016) Toward a quantitative description of radical photoinitiator structure–reactivity correlations. Macromolecules 49:80–89

[45] Yağcı Y, Önen A, Schnabel W (1991) Block copolymers by combination of radical and promoted cationic polymerization routes. Macromolecules 24:4620–4623

[46] Fu K, Huang W, Lin Y, Riddle LA, Carroll DL, Sun YP (2001) Defunctionalization of functionalized carbon nanotubes. Nano Lett 8:439–441

[47] Tucureanu V, Matei A, Avram AM (2016) FTIR spectroscopy for carbon family study. Crit Rev Anal Chem 46:502–520

[48] Ma PC, Kim JK (2011) Carbon nanotubes for polymer reinforcement. CRC Press, Boca Raton

[49] Jorio A, Pimenta MA, Filho AGS, Saito R, Dresselhaus G, Dresselhaus MS (2003) Characterizing carbon nanotube samples with resonance raman scattering. New J Phys 139:1–17

[50] Datsyuk V, Kalyva M, Papagelis K, Parthenios J, Tasis D, Siokou A, Kallitsis I, Galiotis C et al (2008) Chemical oxidation of multiwalled carbon nanotubes. Carbon 46:833–840

[51] Zhaoa Z, Yanga Z, Huc Y, Li J, Fana X (2013) Multiple functionalization of multi-walled carbon nanotubes with carboxyl and amino groups. Appl Surf Sci 276:476–481